



Use of amorphous Nb₂O₅ and Nb₂O₅/Al₂O₃ as acid catalysts for the dehydration of xylose to furfural

Letícia Franzo de Lima¹ · Julia Letícia Montanari Lima¹ ·
Diogo Silva Sanches Jorqueira¹ · Richard Landers² · Silvia Fernanda Moya¹ ·
Raphael Soeiro Suppino¹

Received: 13 October 2020 / Accepted: 7 January 2021 / Published online: 31 January 2021
© Akadémiai Kiadó, Budapest, Hungary 2021

Abstract

This work compared the catalytic performance of the amorphous Nb₂O₅ (NB) and 12 wt% Nb₂O₅/Al₂O₃ (NB-AL) catalysts for the xylose dehydration to furfural carried out for 6 h at 140 and 160 °C using water or a 1:0.8 (v/v) water/isopropanol mixture as solvents. The solids were characterized by XRD, N₂ adsorption, TGA, XPS, TPD-NH₃ and FTIR-Pyridine. Results indicated a specific surface area of 144 and 108 m²/g and an average pore diameter of 44 and 76 Å to NB and NB-AL respectively. The solids presented similar density of acid sites (6.0 for NB and 5.7 μmolNH₃/m² for NB-AL), but different strength distribution of the acid sites. Moreover, the fraction of Brønsted acid sites on NB was 27%, whereas on NB-AL it was only 2%. Concerning the catalytic tests, the highest conversion of xylose for NB and NB-AL (99.0 and 91.1%, respectively) was achieved for the reactions at 160 °C in water/isopropanol mixture, whilst the highest selectivities to furfural were obtained in reactions with water at 160 °C (60.1% to NB and 35.1% to NB-AL). Finally, using water as solvent, the selectivity to furfural increased with both catalysts at the highest temperature, though the carbon balance decreased.

Keywords Xylose dehydration · Niobium oxide · Furfural · Acid catalysis · Supported catalyst · Isopropanol

Supplementary Information The online version contains supplementary material available at <https://doi.org/10.1007/s11144-021-01931-y>.

✉ Letícia Franzo de Lima
lelima89@hotmail.com

¹ Department of Process Engineering, School of Chemical Engineering, University of Campinas, 500, Albert Einstein Avenue, Campinas, SP CEP: 13083-852, Brazil

² Department of Applied Physics, Gleb Wataghin Institute of Physics, University of Campinas, 777, Sérgio Buarque de Holanda Street, Campinas, SP CEP: 13083-859, Brazil

Introduction

The current growing energy demand and the negative effects of burning fossil fuels are increasingly encouraging the use of renewable energy sources [1]. Among the main sources of renewable raw material, lignocellulosic biomass (LB) stands out and its catalytic conversion has been subject of several studies during the last decade.

Lignocellulosic biomass (LB) is obtained from agricultural residues, aquatic plants and wood with structure mainly composed of lignin, cellulose and hemicellulose [2]. Hemicellulose derivatives appear as a very important raw material for synthesizing green chemicals. Hemicellulose is an amorphous heteropolymer whose components are mostly xylan and lesser amounts of arabinan, glucan, mannan, galactan, acetic acid, and uronic acids [2]. Xylose constitutes between 3 and 30% of LB [3] and can be transformed into furfural, furfuryl alcohol, xylitol, tetrahydrofuran, levulinic acid, ethylene glycol, among others important building blocks for current chemical industry.

Furfural (2-furaldehyde) is currently obtained through the dehydration of xylose and has an average production of 250,000 tons per year of which about 70% are produced in China [4]. It is an excellent solvent for organic materials, such as resins and polymers, as well as it can be used as a raw material for the production of gasoline, diesel and airplane fuel [5]. Therefore, the use of heterogeneous catalysis in the production of furfural has emerged as an alternative to the traditional process (carried out through homogeneous catalysis) due to issues like low furfural yield, high energy demand, severity of process conditions and the impressive amount of effluents generated on homogeneous processes [6].

Solid catalysts applied in the production of furfural come from several sources: silicas [7, 8], zeolites [9–12], phosphates [13–15], oxides [16–19] and others. The two possible reaction routes for xylose dehydration to furfural are shown in Fig. 1. Studies reported that Catalysts with a greater amount of Brønsted acid sites (BAS) favors the direct route for the formation of furfural, while the presence of Lewis acid sites (LAS) promotes the isomerization of xylose (indirect route) [20–22]. Weingarten et al. [23] demonstrated that higher amounts of LAS led to the formation of by-products from xylose and lower yields to furfural. Moreover, You et al. [24] pointed out the formation of C_1 – C_3 products and isomers from xylose in the presence high content of LAS. Indeed, even in similar reactions, such as glucose conversion from 5-HMF, the medium to strong LAS decreased the selectivity to the main product [25] and an optimum ratio of BAS and LAS sites was necessary [26].

The oxides derived from niobium have been studied in this reaction [27–29] due to their high surface acidity. In contrast, studies have shown that the high density of acid sites can lead to a decrease in the activity of catalysts due to the large formation of humins [30]. In this way, the use of niobium-based supported catalysts in this reaction aims to decrease the density of the acid sites on the solid surface by dispersing niobium species onto a high surface support. Hence, less humins formation and greater catalyst stability are sought.

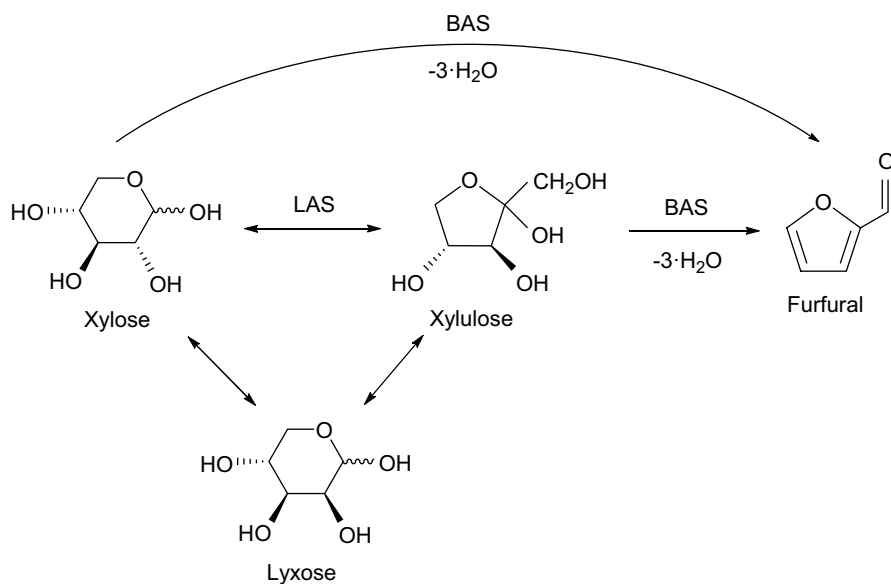


Fig. 1 Reaction pathways for converting xylose to furfural. Source: adapted from [21, 22]—reproduced with the permission of ACS

Generally water is used as solvent because it has the capacity of releasing H^+ in reaction media [31]. Also, recent literature researches reported that the formation of humins can also be reduced through the use of co-solvents, such as toluene, γ -valerolactone, isopropanol (IPA) among others [28, 32]. Their role is to affect the dispersion and conversion of xylose, as well as the formation, distribution, degradation and separation of furfural [33]. With regards to IPA, it may develop hydrogen bonds in furfural molecule, increasing solubilization [33]. Moreover, it is one of the most promising solvents derived from green routes.

Hence, in this study the performance of amorphous niobium oxide (Nb_2O_5) and niobium oxide supported on $\gamma\text{-Al}_2\text{O}_3$ are assessed in the dehydration reaction of xylose to furfural in the presence of water or a water/isopropanol mixture as solvents.

Experimental

Catalyst preparation

Niobic acid ($\text{Nb}_2\text{O}_5 \cdot n\text{H}_2\text{O}$ —Companhia Brasileira de Metalurgia e Mineração, 77.4%) was calcined at 300°C for 4 h under synthetic air flow (80 mL/min) with a heating rate of $10^\circ\text{C}/\text{min}$. This solid was labelled NB.

For the preparation of 12 wt% $\text{Nb}_2\text{O}_5/\text{Al}_2\text{O}_3$, the $\gamma\text{-Al}_2\text{O}_3$ support (Alfa Aesar, 99.99%) was previously calcined at 550°C for 6 h under the same conditions applied for NB. The wet impregnation method was adapted from the procedure described

by Kitano et al. [34]. The impregnation was conducted using a rotary evaporator (IKA—RV 10 control). The Nb precursor used was ammoniacal niobium oxalate ($\text{NH}_4\text{NbO}(\text{C}_2\text{O}_4)_2 \cdot (\text{H}_2\text{O})_n$ —Sigma-Aldrich, 99.99%). Precursor and support were kept for 2 h under stirring with distilled water at 80 °C. After this time, vacuum was applied until almost all water evaporated. Subsequently, the solid was dried in an oven at 80 °C for 12 h. Finally, the solid was calcined at 400 °C for 4 h (synthetic air flow – 80 mL/min). This was labelled NB-AL.

Catalysts characterization

Powder X-ray diffraction (XRD) measurements were performed with a Philips Analytical X-Ray (X'Pert-MPD) with Cu K α radiation of 1.54056 Å. The 2 θ scanning range was from 20° to 80° (0.02° step, 0.50 s/step).

In N₂ adsorption–desorption experiments, the solids were analyzed using a Micromeritics ASAP 2010 apparatus. The samples were previously treated under vacuum at 105 °C for 12 h. Subsequently, the catalysts were cooled to – 196 °C under 3 μmHg pressure. The data interpretation was performed by Brunauer–Emmett–Teller (BET) [35] and Barrett–Joyner–Halenda (BJH) [36] models for the specific surface area and pore size distribution, respectively. Thermal gravimetric analyses (TGA) were performed on the non-calcined samples in a TGA analyzer from SHIMADZU (TGA-50 M), with a scan of 10 °C/min, from 25 to 900 °C under synthetic air flow (50 mL/min). In order to better identify the thermal events that occurred, derivative thermogravimetry (DTG) and differential scanning calorimetry (DSC) were also calculated.

The X-ray photoelectron spectroscopy (XPS) analyses were carried out with a spherical VSW HA-100 analyzer with an aluminum anode (Al K α , $h\nu = 1486.6$ eV). To correct binding energies, the line C 1s (284.6 eV) were used as reference for NB-AL and NB.

To analyze the acidity strength of the catalysts, the temperature-programmed desorption of ammonia (TPD-NH₃) was carried out. The used apparatus was a Micromeritics AutoChem II 2920. Initially, the samples were pretreated under a helium atmosphere at 300 °C (increment of 10 °C/min and flow rate of 25 mL/min). The samples were then cooled down to about 50 °C and subjected to ammonia flow for 30 min. The physisorbed ammonia was removed by purging the system for 30 min under helium flow. The desorption was carried out under helium flow up to 650 °C with heating rate of 10 °C/min and it was monitored using a thermal conductivity detector (TCD).

FTIR spectra of adsorbed pyridine (FTIR-Py) were recorded on a Thermo Scientific Nicolet 6700 FT-IR spectrometer. Each spectrum was analyzed over 128 scans between 4000 and 1000 cm^{-1} with a resolution of 2 cm^{-1} . Self-supporting wafers of the samples were placed in a vacuum cell with a KBr window. The catalyst surfaces were evacuated under a 2.10^{-5} mbar dynamic vacuum for 2 h at 150 °C (NB) or 14 h at 250 °C (NB-AL). After that, they were exposed to pyridine vapor and degassed at different temperatures (100, 200 and 300 °C) to measure the strength of

the sites (weak, medium and strong, respectively) [37]. The extinction coefficients were $I_L = 1.1 \text{ cm}/\mu\text{mol}$ and $I_B = 0.73 \text{ cm}/\mu\text{mol}$ [38].

Catalytic tests

The xylose dehydration reaction was carried out in a semi-batch Parr reactor at 140 or 160 °C under stirring (700 rpm). An inert atmosphere (N_2 , 4.0 MPa) was kept in order to maintain the reaction medium in the liquid phase. The amount of xylose (D-(+)-xylose, Sigma-Aldrich, $\geq 99.9\%$) was sufficient to maintain the concentration of 20 g/kg (200 mL total solution). Catalyst/substrate ratio of 20% (w/w) was used in all reactions performed [39]. Catalytic tests were carried out for 6 h using either deionized water or a 1:0.8 (v/v) deionized water/isopropanol mixture as reaction medium.

The samples were quantified using Waters 717 plus Autosamples High Performance Liquid Chromatography. The detector used was the Waters 410 Differential Refractometer and the Phenomenex Rezex RHM Monosaccharide H+ column was applied with a mobile water phase (flow rate of 0.6 mL/min) at 80 °C. The parameters used to evaluate the performance of the catalysts were: conversion of xylose (X), selectivity to furfural (S), furfural yield (Y) and carbon balance (CB), as shown on Eqs. (1–4), where n_c is the numbers of carbon atoms in each molecule and N_i is the number of moles of the i component.

$$X = \frac{[\text{xylose}]_0 - [\text{xylose}]_t}{[\text{xylose}]_0} \quad (1)$$

$$S = \frac{[\text{furfural}]_t}{[\text{xylose}]_0 - [\text{xylose}]_t} \quad (2)$$

$$Y = \frac{[\text{furfural}]_t}{[\text{xylose}]_0} \quad (3)$$

$$CB = \frac{N_{\text{xylose}} \times 5 + \sum N_{\text{product}} \times n_c}{N_{\text{xylose}_0} \times 5} \quad (4)$$

Results and discussion

Catalyst characterization

XRD analysis of NB and NB-AL catalysts are shown in Fig. 2. From diffractograms it is possible to infer that NB structure is a predominantly non-crystalline [19]. Hence, one may conclude that the calcination treatment conditions were adequate to

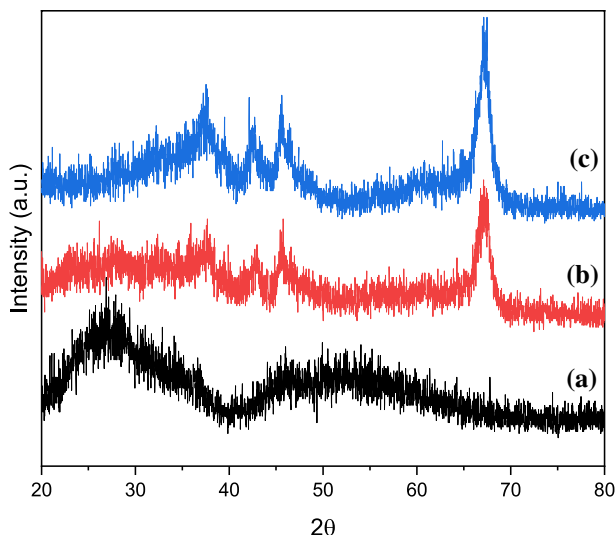


Fig. 2 XRD diffractograms of *a* NB, *b* NB-AL and *c* γ - Al_2O_3

prevent crystallization of Nb_2O_5 . This characteristic is also present in other studies with the same material [40–43].

In turn, the γ - Al_2O_3 diffractogram presents characteristic peaks at 37.4° , 39.7° , 42.8° , 45.8° , 60.5° and 67.3° (2θ) attributed to γ -phase alumina (JCPDS 4-0880). Moreover, the XRD spectrum indicates that this material is also predominantly non-crystalline, hence, a suitable support to be used in the synthesis of solid catalysts [19].

The NB-AL diffractograms did not show any evident alterations in comparison to the support diffractograms. This was probably due to the amount of niobium oxide supported on alumina (only 12 wt%) [19]. García-Sancho et al. [39] reported that the absence of characteristic peaks of the Nb_2O_5 phases in supported catalysts is due to the presence of amorphous particles or small niobium oxide crystalline domains over catalyst surface.

Kitano et al. [44] evaluated the $\text{Nb}_2\text{O}_5/\text{Al}_2\text{O}_3$ catalyst with similar niobium oxide loading. They observed that until the calcination temperature of 850°C its structure presents a profile very similar to the one shown in Fig. 2 (NB-AL). Besides, studies of the same research group reported the formation of AlNbO_4 with Nb_2O_5 contents higher than 16 wt% in Al_2O_3 support after the calcination at 850°C [45]. Jiao et al. [46] evaluated the impregnation of Nb_2O_5 in γ - Al_2O_3 in the range of 1–40 wt%. They concluded that only above a load of 25 wt% of Nb_2O_5 it is possible to verify some characteristic peaks of crystalline niobium oxide (region between 22° and 29°).

The average pore diameters values of NB, NB-AL and γ - Al_2O_3 presented in Table 1 suggests that all solids can be considered as mesoporous [47]. The values obtained in this study were similar to others with similar materials [42, 44, 48]. Both catalysts showed textural properties that may allow xylose to access active sites,

Table 1 Specific surface area, pore volume and average pore diameter of NB, γ -Al₂O₃ and NB-AL

| Sample | Specific surface area (m ² /g) | Pore volume (cm ³ /g) | Average pore diameter (Å) |
|--|---|----------------------------------|---------------------------|
| NB | 142 | 0.16 | 44 |
| γ -Al ₂ O ₃ | 95 ^a | 0.25 | 106 ^a |
| NB-AL | 108 ^a | 0.21 | 76 ^a |

^aValues obtained from Lima et al. [19]

once the average pore diameters of 44 and 76 Å for NB and NB-AL, respectively, could guarantee the diffusion of xylose (6.8 Å) and furfural (5.7 Å) to acid sites. In addition, their high specific surface areas may provide an effective availability of sites for the reaction to occur.

NB-AL catalyst had an increase of its specific surface area compared to the support. This increase possibly occurred due to niobium oxides that formed on the material surface [44]. Despite this, the measurement of average pore volume and diameter decreased. This observation indicates that during impregnation of niobium oxide precursor, agglomerates were formed on support surface, causing partial blockage of its pores. The results agree with the Nb₂O₅ impregnation observed by Kitano et al. [44].

TG analysis of NB catalyst precursor, Nb₂O₅·nH₂O (Fig. 3a), exhibited total mass loss of 19.3% up to 250 °C. This event was expected, once a significant water content of water in the niobic acid was reported by the manufacturer. Besides, the exothermic event around 550 °C in the DSC curve may indicate the crystallization process of amorphous niobium oxide [49]. Then, in order to avoid crystallization of the material and loss of surface area and acidity, catalyst calcination temperature should not exceed 500 °C [50]. Therefore, after the result presented by the TGA analysis, the calcination temperature of 300 °C was selected to ensure that all mass loss events have already ended.

Concerning to the NB-AL solid, the main mass loss event verified by TGA of NB-AL (Fig. 3b) was between 213 and 339 °C. According to Medeiros et al. [51] and Su et al. [52], this event can be attributed to decomposition of oxalate niobium

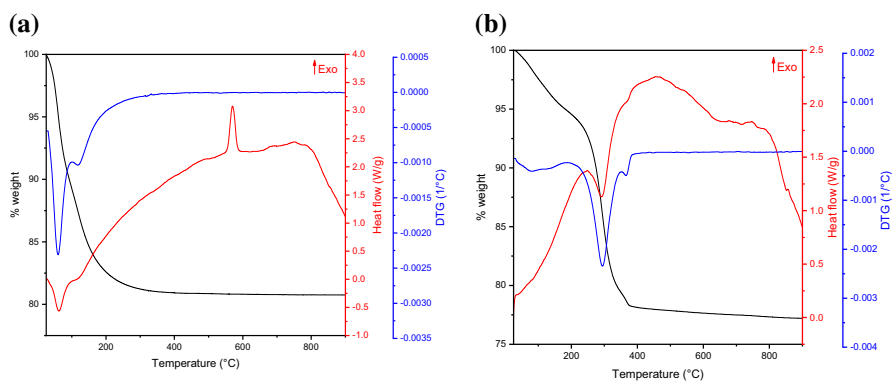


Fig. 3 Thermogravimetric analysis (TGA, DSC and DTG) of the non-calcined **a** NB and **b** NB-AL

precursor and consequently formation of niobium oxide. In fact, it is important to note that the calcination temperature to which this catalyst was subjected (400 °C) was defined after TGA analysis and was sufficient to remove all precursors salt anions from the catalyst surface [51, 52] without further degradation of catalyst structure.

XPS results presented in Table 2 were compared with several studies in order to identify catalysts surface species. For the catalyst NB, the peak with binding energy 207.69 eV (Entry 1) can be attributed to niobium pentoxide. In addition, the surface Nb/O ratio of 29/71 is exactly the theoretical value for the atomic composition of the stoichiometric Nb₂O₅.

For NB-AL catalyst, binding energy of 74.45 eV measured (Entry 6) is characteristic of aluminum in gamma phase of aluminum oxide (γ -Al₂O₃) [39, 53]. Furthermore, two niobium oxide species were found at NB-AL catalyst surface. At 207.14 eV (Entry 5) the peak can be attributed to niobium in Nb₂O₅ structure [54]. Moreover, it was observed a binding energy of 204.79 eV (Entry 4), which was not matched with any other value in literature. Some studies have identified evidence of the formation of a second niobium structure on the alumina surface after the impregnation process [55–57]. Kitano et al. [57] reported that the NbO₆ structures of niobium oxide can be distributed randomly along the surface, which could cause interfaces of overlapping layers. They also exposed the possibility of aggregating niobium oxide to form a new structure (AlNbO₄). Although the conditions for preparing the catalyst in this study are milder than that presented by Kitano et al. [57], it is possible that there were regions of heterogeneous distribution on the NB-AL surface, which generated the formation of this second structure with lower binding energy. However, the formation of aluminum niobate is unlikely due to lower temperatures than used (calcination of 400 °C for NB-AL).

The O 1s binding energies in NB were 530.71 (entry 2) and 532.58 eV (entry 3). These values refer to the bond between niobium and oxygen on the catalytic surface. De Pietre et al. [58] reported that in niobic acid, the Nb–O bond has a binding energy of 530.4 and the double bond Nb=O bond has 532.3 eV [58].

Table 2 XPS analysis of NB and NB-AL catalysts

| Entry | Catalyst | Element | Binding energy (eV) | Atomic composition (%) | | | Nb/Al |
|-------|----------|----------------------|---------------------|------------------------|----|----|-------|
| | | | | Nb | O | Al | |
| 1 | NB | Nb 3d _{5/2} | 207.69 | 29 | 71 | – | – |
| 2 | | O 1s | 530.71 | | | | |
| 3 | | O 1s | 532.58 | | | | |
| 4 | NB-AL | Nb 3d _{5/2} | 204.79 | 5 | 60 | 35 | 0.14 |
| 5 | | Nb 3d _{5/2} | 207.14 | | | | |
| 6 | | Al 2p _{3/2} | 74.45 | | | | |
| 7 | | O 1s | 529.77 | | | | |
| 8 | | O 1s | 531.24 | | | | |
| 9 | | O 1s | 533.06 | | | | |

The catalyst NB-AL presented three different binding energies for oxygen. The peak with center at 529.77 eV (entry 7) refers to niobium pentoxide [59], while the peak with center 531.24 eV (entry 8) refers to the bond between oxygen and aluminum in Al_2O_3 [60]. The third peak with energy 533.06 eV (entry 9) was not matched with any other value in literature. Possibly it is related to the bond between oxygen and the niobium that presented energy of 204.79 eV (entry 4) constituting the second niobium structure on the alumina surface.

The atomic surface Nb content in NB-AL indicated by the XPS (5%) was higher than the nominal value (1.9%). The niobium oxide monolayer on the surface of the alumina is formed only when the mass percentage of 16% Nb_2O_5 is reached [57]. Although the niobium oxide monolayer on the surface of the alumina has not been completely formed, this is an indication that the Nb_2O_5 is well dispersed onto the surface. Furthermore, the amount of Nb in the surface was confirmed due to Nb/Al ratio of 0.14 (last column of Table 2). Similar value was obtained by recent studies involving supported $\text{Nb}_2\text{O}_5/\gamma\text{-Al}_2\text{O}_3$ solids with a mass percentage close to that of this study [45].

In the study of the total acidity of the solids by TPD- NH_3 (Table 3), the classification of site strength followed the study of Marciver et al. [61] and Berteau and Delmon (1989) [62]: from 25 to 200 °C (weak acid sites), from 200 to 400 °C (medium acid sites) and from 400 to 500 °C (strong acid sites). For further information, the TPD- NH_3 profiles of NB, $\gamma\text{-Al}_2\text{O}_3$ and NB-AL are presented in Fig. S1 (Supplementary Material) and the force distribution of the acid sites is shown in Fig. 4.

The NB catalyst showed a total acidity of 859.3 $\mu\text{molNH}_3/\text{g}$ (Table 3, Entry 1) distributed more intensely among weak and medium strength acid sites. For $\gamma\text{-Al}_2\text{O}_3$ support total acidity was 530.6 $\mu\text{molNH}_3/\text{g}$ (Table 3, Entry 2), which is consistent with García-Sancho et al. [39] that present a similar value of acidity 543.5 $\mu\text{molNH}_3/\text{g}$ for γ -alumina. Finally, as expected, after the impregnation process, new acid sites were added on the support surface. This resulted in an increase of acidity of almost 20% (from 530.6 to 617.8 $\mu\text{molNH}_3/\text{g}$) for NB-AL solid. The aforementioned change can be attributed to the possible formation of new niobium clusters on the catalyst surface as verified, for example, by the XPS result. As a result, these new groups increased the strength of sites in all ranges (weak, medium and strong). It is important to note that the catalysts NB and NB-AL had similar density of acid sites (6.0 and 5.7 $\mu\text{molNH}_3/\text{m}^2$, respectively), though the distribution of acid strength was different. For example, as shown in

Table 3 Amount of NH_3 ($\mu\text{mol}/\text{g}$ and $\mu\text{mol}/\text{m}^2$) desorbed for NB, NB-AL and $\gamma\text{-Al}_2\text{O}_3$

| Entry | Sample | Total acid sites ($\mu\text{molNH}_3/\text{g}$) | Density of acid sites ($\mu\text{molNH}_3/\text{m}^2$) |
|-------|--------------------------------|---|--|
| 1 | NB | 859.3 | 6.0 |
| 2 | $\gamma\text{-Al}_2\text{O}_3$ | 530.6 | 5.5 |
| 3 | NB-AL | 617.8 | 5.7 |

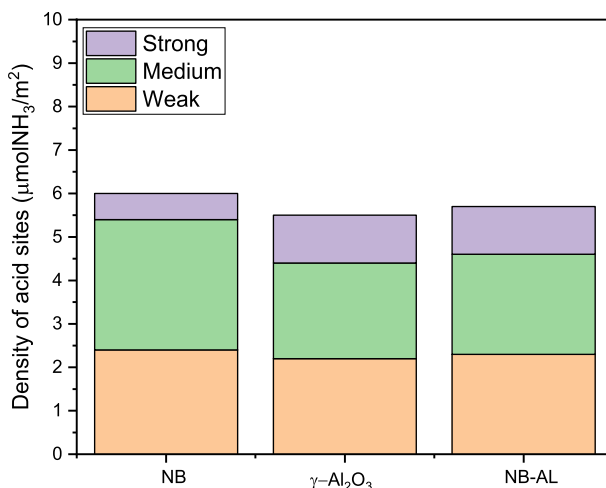


Fig. 4 Amount of NH_3 ($\mu\text{mol}/\text{m}^2$) desorbed for NB, NB-AL and $\gamma\text{-Al}_2\text{O}_3$ as a function of NH_3 desorption temperature (weak < 200 °C; 200 °C $<$ medium < 400 °C; 400 °C $<$ strong < 500 °C)

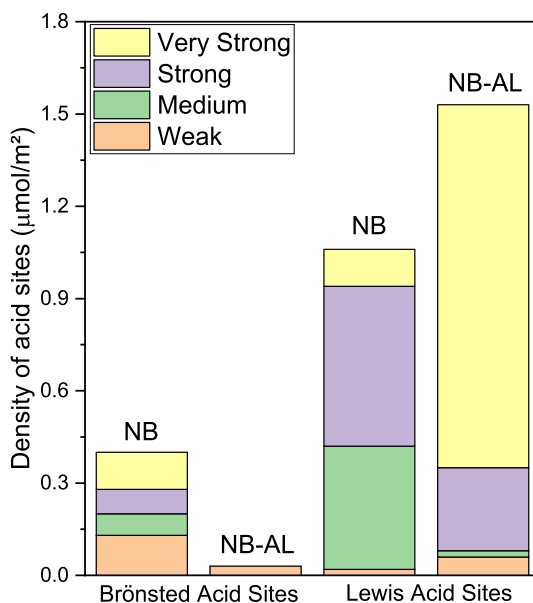
Fig. 4, NB-AL has twice the density of strong acid sites as NB and this will possibly provide different outcomes in their reaction performance.

As mentioned hereinbefore, Lewis acid sites (LAS) may favor an increase in xylose conversion whereas the increase in Brønsted sites (BAS) reflects higher selectivities to furfural [27]. Thus, it is reasonable to look for a catalyst that presents an optimal ratio of the two types of acid sites. FTIR-Py analysis (Fig. S2—Supplementary Material) revealed that NB catalyst has about 27% of Brønsted acid sites (BAS) whilst the NB-AL presented only 2% BAS. Moreover, when compared to the NB catalyst, NB-AL had more contributions of Lewis acid sites: from the support and from the Nb_2O_5 species over surface. This difference of acid sites ratio could directly influence the performance of the catalysts, especially with regards to selectivity.

The force distribution of the BAS and LAS is shown in Fig. 5. It is possible to verify that for NB catalyst the most prominent range of Py-BAS desorption is up to 100 °C (weak sites). Up to that temperature, Brønsted acid sites represent 85% of total (BAS + LAS) weak sites desorbed from surface of Nb catalyst. There is also an intense amount of medium, strong and very strong LAS.

For the supported catalyst (NB-AL), the LAS showed resistance up to 200 °C. This result indicates a major contribution of strong and very strong LAS for total acidity of supported catalyst when compared to the equivalent sites in NB catalyst. Brønsted acid sites are present only up to 100 °C (weak strength) and even so with significantly low concentration. In agreement with results obtained by TPD- NH_3 and by FTIR-Py analysis, can be verified that catalyst total acidity is mainly composed of medium and strong LAS. Therefore, the incorporation of Al_2O_3 (a known Lewis acid solid) into Nb_2O_5 solid led to the decrease of the density of BAS which was only observed as of weak strength while most of LAS were strong and very strong.

Fig. 5 Amount of Py ($\mu\text{mol}/\text{m}^2$) desorbed for NB and NB-AL (weak < 100 °C; 100 °C < medium < 200 °C; 200 °C < strong < 300 °C; very strong > 300 °C)



Both Lewis and Brønsted acid sites are active for the xylose dehydration reaction [21, 22]. Literature reports that the presence of water could hydrolyze the Nb–O–Nb bonds, generating new Brønsted acid sites [37]. Therefore, the catalysts may still undergo changes in their acid sites due to the presence of water inside the reactor. As an example, the transformation into BAS is illustrated at Fig. 6.

Catalytic tests

The catalysts NB and NB-AL were tested in the xylose dehydration reaction for 6 h at two different temperatures (140 and 160 °C) and the solvent system varied from pure water or 1:0.8 (v/v) water/isopropanol mixture. Fig. 7 presents the evolution of the xylose conversion throughout the reaction time for the NB and NB-AL catalysts.

Only xylose and furfural were identified as soluble products through HPLC analysis of reaction mixture using NB catalyst at 160 °C and water as solvent. However, a slight decrease in the catalyst activity was observed after 180 min of reaction (Fig. 7a). The high concentration of acid sites and its specific surface

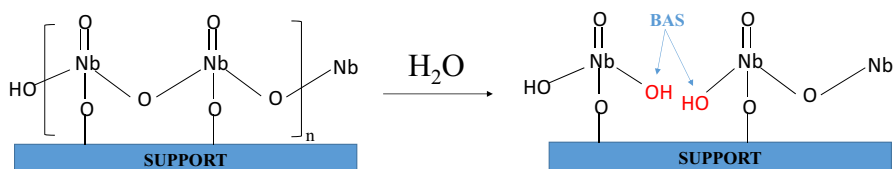


Fig. 6 Possible generation of new Brønsted acid sites in the presence of water. Source: adapted from [37]—reproduced with the permission of Elsevier

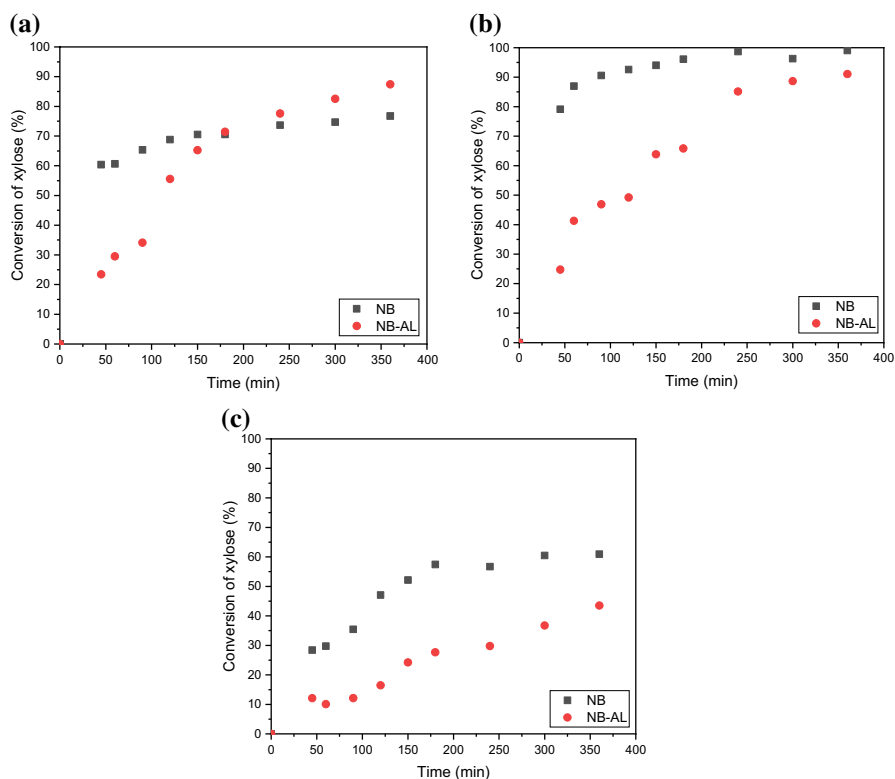


Fig. 7 Conversion of xylose in reactions with **a** water at 160 °C, **b** water/IPA mixture at 160 °C and **c** water at 140 °C. *Reaction conditions:* 4.0 g of xylose, 200 mL of solvent (deionized water or 1:0.8 (v/v) deionized water/isopropanol mixture), 0.8 g of catalyst, N₂ pressure of 4.0 MPa, stirring rate of 700 rpm

area may have favored the formation and deposition of insoluble by-products (such as humins) on the catalyst surface [63]. Over time, humins could block the active acid sites, leading to a decrease of the catalytic activity. A visual qualitative analysis (Table S1—Supplementary Material) of the NB catalyst revealed that the initial white color (fresh catalyst) turns to light brown after the reaction. According to the study of Bernal et al. [64], the dark brown shade can be related to the deposition of humins on the catalyst surface. In addition, the TGA analysis of the fresh and used catalysts (Fig. S3—Supplementary Material) corroborates the hypothesis of humins formation on the surface of the solids. There was a more intense formation of humins in NB-AL than in NB. Weingarten et al. and Pholjaroen et al. highlight that LAS are more active than BAS for reactions that produce humins [13, 23]. This is in agreement with the fact that the higher amount of LAS in NB-AL contributed to a more prominent formation of this by-product. Although NB and NB-AL have similar density of acid sites (Table 3), its surface properties (Table 1) were quite different, since NB has a higher specific surface area and smaller average pore diameter. Even though NB-AL had more humins on

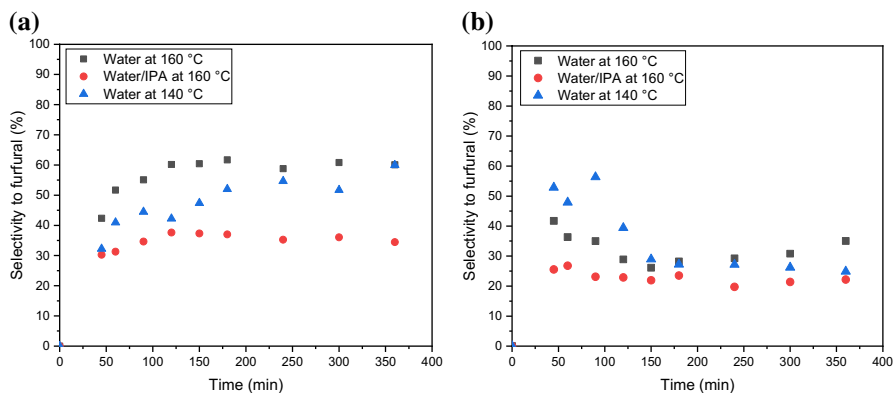


Fig. 8 Selectivity to furfural in the reactions of **a** NB and **b** NB-AL catalysts. Reaction conditions: 4.0 g of xylose, 200 mL of solvent (deionized water or 1:0.8 (v/v) deionized water/isopropanol mixture), 0.8 g of catalyst, N_2 pressure of 4.0 MPa, stirring rate of 700 rpm

Table 4 Conversion of xylose (X), selectivity to furfural (S), furfural yield (Y) and carbon balance (CB) at the end of 6 h of reaction with catalysts NB and NB-AL

| Parameters | Catalyst | | | | | |
|------------|----------|-----------|-------|-------|-----------|-------|
| | NB | | NB-AL | | | |
| T (°C) | 160 | 160 | 140 | 160 | 160 | 140 |
| Solvent | Water | Water/IPA | Water | Water | Water/IPA | Water |
| X (%) | 76.8 | 99.0 | 60.9 | 87.4 | 91.1 | 43.5 |
| S (%) | 60.1 | 34.4 | 59.9 | 35.1 | 22.2 | 24.9 |
| Y (%) | 46.1 | 34.1 | 36.6 | 30.7 | 20.2 | 10.8 |
| CB (%) | 69.3 | 37.8 | 73.1 | 59.2 | 31.8 | 66.4 |

Reaction conditions: 4.0 g of xylose, 200 mL of solvent (deionized water or 1:0.8 (v/v) deionized water/isopropanol mixture), 0.8 g of catalyst, N_2 pressure of 4.0 MPa, stirring rate of 700 rpm

its surface, these factors may have influenced the probable blockage of NB pores, which reflected in the loss of activity.

The reaction with the NB-AL catalyst with water at 160 °C (Fig. 7a) showed four soluble by-products in reaction medium. Then, when compared to NB catalyst at the same temperature (160 °C), the formation of more by-products with the use of NB-AL accounts for the lower selectivity observed in Fig. 8a, b. The values of xylose conversion (X), furfural selectivity (S), furfural yield (Y) and carbon balance (CB) of the end of the reactions are shown at Table 4.

NB-AL catalyst showed lower furfural yields, furfural selectivities and carbon balances compared in relation to NB in all reactions conditions. This was probably due to the fact that the NB-AL had less Brønsted acid sites (2%) than the NB catalyst (27%) [21, 22]. The study of García-Sancho et al. [27] reports that a high percentage of LAS contributes to the increase of the conversion of xylose while a greater amount of BAS reflects an increase in selectivity to furfural. Thus, the results presented by NB and NB-AL are in agreement with the literature.

When the temperature is increased in the reaction medium containing only water, it is possible to observe that the final selectivity to furfural is higher at 160 °C for both catalysts. This indicates that the parallel reactions were not benefited by the temperature rise, unlike the furfural formation reaction. For the NB-AL solid in the reaction at 140 °C, the drop in selectivity observed after ca. 90 min (Fig. 8b) may be attributed to the later formation of by-products, whether they are from parallel reactions of xylose (such as lyxose), or degradation of furfural (e.g., to formic acid, oligomers) [23]. Moreover, comparing the results on Fig. 7a, c, it is noteworthy that an increase on the reaction temperature had significant effects on the xylose conversion of both catalysts. Regardless of the temperature, NB catalyst appears to be more active than NB-AL at the beginning of the reaction.

As previously mentioned, for the reaction system containing NB-AL and water 160 °C four by-products were observed, among which lyxose was identified. This same by-product was also present in the reactions with NB catalyst with water/IPA at 160 °C and with water at 140 °C. The selectivity curves of lyxose are shown in Fig. 9.

It should be noted here that, according to Gallo et al. [10], lyxose and xylulose isomers are not easily separated through liquid chromatography. For the reaction of NB-AL in water 160 °C at about 150 min the selectivity to lyxose decreases (Fig. 9) whilst the selectivity to furfural increases (Fig. 8b). This possibly occurs due to the consumption of this xylose isomer for the formation of furfural via the indirect reaction route.

Higher values of furfural yield were also observed for the reactions at higher temperature and this indicate that high temperatures had more beneficial effects in relation to the performance of both catalysts, which is in agreement with previous

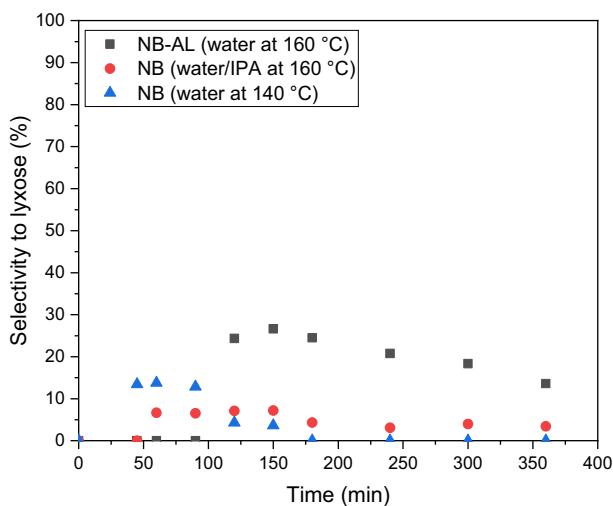


Fig. 9 Selectivity to lyxose. Reaction conditions: 4.0 g of xylose, 200 mL of solvent (deionized water or 1:0.8 (v/v) deionized water/isopropanol mixture), 0.8 g of catalyst, N₂ pressure of 4.0 MPa, stirring rate of 700 rpm

works [15, 27, 65, 66]. Conversely, the carbon balance decreased at higher temperatures, probably due to the increase of reaction rates in parallel reactions. As the soluble and insoluble by-products could not be identified and quantified due to the broad spectra of side products in furfural production, the carbon balance presented most values close to 60 and 70%. Conversely, in water/IPA reactions, those results decreased to about 30 and 40%.

The use of isopropanol as a co-solvent led to a drastic increase of catalytic activity for NB catalyst. As seen on Fig. 7b, a complete conversion of xylose was achieved at ca. 200 min with this catalyst, whereas without isopropanol a maximum conversion of ca. 75% was achieved after 360 min at the same temperature (160 °C). In turn, the presence of isopropanol had little effect on the activity of NB-AL. Recently, Molina et al. [28] reported that isopropanol increased the activity of niobium oxide based-catalysts. Then, the catalytic tests carried out with water/IPA as reaction medium reached higher conversions than the ones containing only water. According to literature, the alcohol solubilizes some of the by-products formed and decreases the amount of insoluble products over catalyst surface, ensuring higher stability, and consequent activity to the catalyst [28]. In turn, the lower values of selectivity to furfural observed in the presence of IPA (Fig. 8) may be attributed to the increase in the formation of soluble by-products from degradation of xylose and furfural [28, 33]. When comparing the mass loss values of the catalysts used (Fig. S2) it is possible to observe evidence of a smaller amount of solid material accumulated on the surface of the catalysts used in the reactions with isopropanol. This result corroborates with that presented in the literature, which points out that in reactions with water only, the formation of this insoluble by-product is greatly favored [67].

Table 5 summarizes the results obtained with niobium-based catalysts for xylose dehydration in this work compared to other studies.

When the catalysts of this study (lines 6–9) are compared to similar systems in the literature, the results of conversion are similar to reactions with 24 h (entries 2 and 3). This demonstrates the high activity of the systems, especially for NB catalyst with BAS high content, which exhibited excellent selectivity in water (60.1% at line

Table 5 Comparison of NB and NB-AL catalytic performance with other systems reported in the specialized literature

| Entry | Catalyst | Solvent | Reaction time (min) | T (°C) | X (%) | S (%) | References |
|-------|---|---------------|---------------------|--------|-------|-------|------------|
| 1 | NbP | Water | 60 | 160 | 44.1 | 39.5 | [13] |
| 2 | 12 wt% Nb ₂ O ₅ /SBA-12 | Water/toluene | 1440 | 160 | 85.0 | 93.0 | [39] |
| 3 | 12 wt% Nb ₂ O ₅ /MCM-41 | Water/toluene | 1440 | 160 | 80.0 | 84.0 | [39] |
| 4 | 12 wt% Nb ₂ O ₅ /Al ₂ O ₃ | Water/toluene | 240 | 160 | 62.0 | 59.0 | [39] |
| 5 | Nb ₂ O ₅ | Water/toluene | 90 | 170 | 90.0 | 56.0 | [27] |
| 6 | NB | Water | 360 | 160 | 76.8 | 60.1 | This work |
| 7 | NB | Water/IPA | 360 | 160 | 99.0 | 34.4 | This work |
| 8 | NB-AL | Water | 360 | 160 | 87.4 | 35.1 | This work |
| 9 | NB-AL | Water/IPA | 360 | 160 | 91.1 | 22.2 | This work |

6). Indeed, the selectivity of this solid was higher than the niobium oxide catalyst in water/toluene system (56%, at line 5). Then, the use of water as a solvent is promising for NB catalyst, once it is less aggressive to the environment than the organic solvents.

Conclusions

Results presented in this work show that the Nb_2O_5 catalyst had better performance on its pure form (NB) than the $\text{Nb}_2\text{O}_5/\gamma\text{-Al}_2\text{O}_3$ (NB-AL) for the xylose dehydration to furfural in all reaction conditions.

Both catalysts presented similar textural properties and were predominantly amorphous, given that calcination conditions were adequate to form niobium oxides and also prevent their crystallization. Acidity studies revealed that whereas both solids presented similar values of density of acid sites, though the distribution of acid sites strength and types were different. NB solid Brønsted acid sites ca. 13 times higher than for NB-AL. This led to different performances in xylose dehydration.

Whilst both solids were active for the dehydration of xylose to furfural, the performance of NB catalyst was remarkably superior with maximum selectivity to furfural of 60% against 35% of NB-AL. The presence of isopropanol in the reaction medium led to an increase in the conversion of xylose. However, the furfural selectivity, yield of furfural, carbon balance and formation of humins decreased. The intense amount of non-quantified by-products contributed to the low carbon balance values.

Acknowledgements The author authors thank the financial supported by the “National Council for Scientific and Technological Development—CNPq” (Process 142364/2016-9) and “São Paulo Research Foundation—FAPESP” (Process no. 2018/20532-0). This study was financed in part by the Coordenação de Aperfeiçoamento de Pessoal de Nível Superior—Brasil (CAPES)—Finance Code 001.

Author contributions LFDL: conceptualization, methodology, investigation, writing—original draft, visualization, project administration. JLML: investigation. diogo silva sanches jorqueira: writing—review and editing. RL: investigation, resources. SFM: conceptualization, writing—review and editing, supervision. RSS: conceptualization, resources, writing—review and editing, supervision, project administration.

Funding This work is financially supported by the “National Council for Scientific and Technological Development—CNPq” (Process 142364/2016-9) and “São Paulo Research Foundation—FAPESP” (Process no. 2018/20532-0). This study was financed in part by the Coordenação de Aperfeiçoamento de Pessoal de Nível Superior—Brasil (CAPES)—Finance Code 001. This work has also been supported by the “National Council for Scientific and Technological Development—CNPq” (Universal Call MCTIC/CNPq 28/2018 process no. 431272/2018-2) and was conducted within the scope of grant #2015/20630-4, São Paulo Research Foundation (FAPESP).

Data availability The raw/processed data required to reproduce these findings cannot be shared at this time as the data also forms part of an ongoing study.

Compliance with ethical standards

Conflict of interest The authors declare that they have no known competing financial interests or personal relationships that could have appeared to influence the work reported in this paper.

Informed consent The authors declare that they are in agreement with the participation in this study. The authors declare that they are in agreement with the publication of this study.

References

1. Bajwa DS, Peterson T, Sharma N et al (2018) A review of densified solid biomass for energy production. *Renew Sustain Energy Rev* 96:296–305. <https://doi.org/10.1016/j.rser.2018.07.040>
2. Cai CM, Zhang T, Kumas R, Wyman CE (2014) Integrated furfural production as a renewable fuel and chemical platform from lignocellulosic biomass. *J Chem Technol Biotechnol* 89:2–10. <https://doi.org/10.1002/jctb.4168>
3. Gírio FM, Fonseca C, Carvalheiro F et al (2010) Hemicelluloses for fuel ethanol: a review. *Bioreour Technol* 101:4775–4800. <https://doi.org/10.1016/j.biortech.2010.01.088>
4. Mishra RK, Kumar VB, Victor A et al (2019) Selective production of furfural from the dehydration of xylose using Zn doped CuO catalyst. *Ultrason Sonochem* 56:55–62. <https://doi.org/10.1016/j.ultsonch.2019.03.015>
5. Weingarten R, Cho J, Conner WC Jr, Huber GW (2010) Kinetics of furfural production by dehydration of xylose in a biphasic reactor with microwave heating. *Green Chem* 12:1423–1429. <https://doi.org/10.1039/c003459b>
6. Win DT (2005) Furfural: gold from garbage. *Assumpt Univ J Technol* 8:185–190
7. Agirrezabal-Telleria I, Requies J, Güemez MB, Arias PL (2014) Dehydration of d-xylose to furfural using selective and hydrothermally stable arenesulfonic SBA-15 catalysts. *Appl Catal B* 145:34–42. <https://doi.org/10.1016/j.apcatb.2012.11.010>
8. Jeong GH, Kim EG, Kim SB et al (2011) Fabrication of sulfonic acid modified mesoporous silica shells and their catalytic performance with dehydration reaction of d-xylose into furfural. *Microporous Mesoporous Mater* 144:134–139. <https://doi.org/10.1016/j.micromeso.2011.04.002>
9. Lima S, Pillinger M, Valente AA (2008) Dehydration of d-xylose into furfural catalysed by solid acids derived from the layered zeolite Nu-6(1). *Catal Commun* 9:2144–2148. <https://doi.org/10.1016/j.catcom.2008.04.016>
10. Gallo JMR, Alonso DM, Mellmer MA et al (2013) Production of furfural from lignocellulosic biomass using beta zeolite and biomass-derived solvent. *Top Catal* 56:1775–1781. <https://doi.org/10.1007/s11244-013-0113-3>
11. Kaiprommarat S, Kongparakul S, Reubroycharoen P et al (2016) Highly efficient sulfonic MCM-41 catalyst for furfural production: furan-based biofuel agent. *Fuel* 174:189–196. <https://doi.org/10.1016/j.fuel.2016.02.011>
12. Iglesias J, Melero JA, Morales G et al (2016) Dehydration of xylose to furfural in alcohol media in the presence of solid acid catalysts. *ChemCatChem* 8:2089–2099. <https://doi.org/10.1002/cctc.201600292>
13. Pholjaroen B, Li N, Wang Z et al (2013) Dehydration of xylose to furfural over niobium phosphate catalyst in biphasic solvent system. *J Energy Chem* 22:826–832. [https://doi.org/10.1016/S2095-4956\(14\)60260-6](https://doi.org/10.1016/S2095-4956(14)60260-6)
14. Zhu Y, Kanamori K, Brun N et al (2016) Monolithic acidic catalysts for the dehydration of xylose into furfural. *Catal Commun* 87:112–115. <https://doi.org/10.1016/j.catcom.2016.09.014>
15. Fang C, Wu W, Li H et al (2017) Production of bio-based furfural from xylose over a recyclable niobium phosphate (NbOPO₃) catalyst. *Energy Sources A* 39:2072–2077. <https://doi.org/10.1080/15567036.2017.1402103>
16. García-Sancho C, Sádaba I, Moreno-Tost R et al (2013) Dehydration of xylose to furfural over MCM-41-supported niobium-oxide catalysts. *Chemsuschem* 6:635–642. <https://doi.org/10.1002/cssc.201200881>
17. Moreno-Marroán C, Barbaro P, Caporali S, Bossola F (2018) Low-temperature continuous-flow dehydration of xylose over water-tolerant niobia-titania heterogeneous catalysts. *Chemsuschem* 11:3649–3660. <https://doi.org/10.1002/cssc.201801414>
18. Gómez Millán G, El Assal Z, Nieminen K et al (2018) Fast furfural formation from xylose using solid acid catalysts assisted by a microwave reactor. *Fuel Process Technol* 182:56–67. <https://doi.org/10.1016/j.fuproc.2018.10.013>

19. Lima JLM, Lima LF, Moya SF, Suppino RS (2019) Emprego do Catalisador $\text{Nb}_2\text{O}_5/\text{Al}_2\text{O}_3$ na reação de desidratação da xilose a furfural em fase líquida. Anais do Congresso Brasileiro de Iniciação Científica, Uberlândia, pp 1–6
20. Takagaki A, Ohara M, Nishimura S, Ebitani K (2010) One-pot formation of furfural from xylose via isomerization and successive dehydration reactions over heterogeneous acid and base catalysts. *Chem Lett* 39:838–840. <https://doi.org/10.1246/cl.2010.838>
21. Choudhary V, Pinas AB, Sandler SI et al (2011) Xylose isomerization to xylulose and its dehydration to furfural in aqueous media. *ACS Catal* 1:1724–1728. <https://doi.org/10.1021/cs200461t>
22. Choudhary V, Sandler SI, Vlachos DG (2012) Conversion of xylose to furfural using Lewis and Brønsted acid catalysts in aqueous media. *ACS Catal* 2:2022–2028. <https://doi.org/10.1021/cs300265d>
23. Weingarten R, Tompsett GA, Conner WC, Huber GW (2011) Design of solid acid catalysts for aqueous-phase dehydration of carbohydrates: the role of Lewis and Brønsted acid sites. *J Catal* 279:174–182. <https://doi.org/10.1016/j.jcat.2011.01.013>
24. You SJ, Kim YT, Park ED (2014) Liquid-phase dehydration of D-xylose over silica-alumina catalysts with different alumina contents. *React Kinet Mech Catal* 111:521–534. <https://doi.org/10.1007/s11144-013-0655-1>
25. Li X, Peng K, Liu X et al (2017) Comprehensive Understanding of the role of Brønsted and Lewis acid sites in glucose conversion into 5-hydroxymethylfurfural. *ChemCatChem* 9:2739–2746. <https://doi.org/10.1002/cctc.201601203>
26. Pham ST, Nguyen BM, Le GH et al (2020) Role of Brønsted and Lewis acidic sites in sulfonated Zr-MCM-41 for the catalytic reaction of cellulose into 5-hydroxymethyl furfural. *React Kinet Mech Catal*. <https://doi.org/10.1007/s11144-020-01799-4>
27. García-Sancho C, Rubio-Caballero JM, Mérida-Robles JM et al (2014) Mesoporous Nb_2O_5 as solid acid catalyst for dehydration of D-xylose into furfural. *Catal Today* 234:119–124. <https://doi.org/10.1016/j.cattod.2014.02.012>
28. Molina MJC, Granados ML, Gervasini A, Carniti P (2015) Exploitation of niobium oxide effective acidity for xylose dehydration to furfural. *Catal Today* 254:90–98. <https://doi.org/10.1016/j.cattod.2015.01.018>
29. Vieira JL, Almeida-trapp M, Mithöfer A et al (2018) Rationalizing the conversion of glucose and xylose catalyzed by a combination of Lewis and Brønsted acids. *Catal Today*. <https://doi.org/10.1016/j.cattod.2018.10.032>
30. Marzo M, Gervasini A, Carniti P (2012) Improving stability of Nb_2O_5 catalyst in fructose dehydration reaction in water solvent by ion-doping. *Catal Today* 192:89–95. <https://doi.org/10.1016/j.cattod.2011.12.014>
31. Kim SB, Lee MR, Park ED et al (2011) Kinetic study of the dehydration of D-xylose in high temperature water. *React Kinet Mech Catal*. <https://doi.org/10.1007/s11144-011-0320-5>
32. Wang A, Balsara NP, Bell AT (2016) Pervaporation-assisted catalytic conversion of xylose to furfural. *Green Chem* 18:4073–4085. <https://doi.org/10.1039/c6gc00581k>
33. Hu X, Westerhof RJM, Dong D et al (2014) Acid-catalyzed conversion of xylose in 20 solvents: Insight into interactions of the solvents with xylose, furfural, and the acid catalyst. *ACS Sustain Chem Eng* 2:2562–2575. <https://doi.org/10.1021/sc5004659>
34. Kitano T, Shishido T, Teramura K, Tanaka T (2014) Acid property of $\text{Nb}_2\text{O}_5/\text{Al}_2\text{O}_3$ prepared by impregnation method by using niobium oxalate solution: effect of pH on the structure and acid property. *Catal Today* 226:97–102. <https://doi.org/10.1016/j.cattod.2013.09.053>
35. Brunauer S, Emmett PH, Teller E (1938) Adsorption of gases in multimolecular layers. *J Am Chem Soc* 60:309–319. <https://doi.org/10.1021/ja01269a023>
36. Barrett EP, Joyner LG, Halenda PP (1951) The determination of pore volume and area distributions in porous substances. I. computations from nitrogen isotherms. *J Am Chem Soc* 73:373–380. <https://doi.org/10.1021/ja01145a126>
37. García-Sancho C, Cecilia JA, Moreno-Ruiz A et al (2015) Influence of the niobium supported species on the catalytic dehydration of glycerol to acrolein. *Appl Catal B* 179:139–149. <https://doi.org/10.1016/j.apcatb.2015.05.014>
38. Datka J, Turek AMM, Jehng JMM, Wachs IEE (1992) Acidic properties of supported niobium oxide catalysts: an infrared spectroscopy investigation. *J Catal* 135:186–199. [https://doi.org/10.1016/0021-9517\(92\)90279-Q](https://doi.org/10.1016/0021-9517(92)90279-Q)

39. García-Sancho C, Agirrezabal-Telleria I, Güemez MB, Maireles-Torres P (2014) Dehydration of D-xylitol to furfural using different supported niobia catalysts. *Appl Catal B* 152–153:1–10. <https://doi.org/10.1016/j.apcatb.2014.01.013>
40. Iizuka T, Ogasawara K, Tanabe K (1983) Acidic and catalytic properties of niobium pentoxide. *Bull Chem Soc Jpn* 56:2927–2931. <https://doi.org/10.1246/bcsj.56.2927>
41. Brandão RF, Quirino RL, Mello VM et al (2009) Synthesis, characterization and use of Nb₂O₅ based catalysts in producing biofuels by transesterification, esterification and pyrolysis. *J Braz Chem Soc* 20:954–966
42. Avila AJ, Tonetto GM, Damiani DE (2011) Acidolysis of tripalmitin with capric acid using Nb₂O₅ and MgO as heterogeneous catalysis. *Catal Commun* 12:362–367. <https://doi.org/10.1016/j.catcom.2010.10.007>
43. Chan X, Pu T, Chen X et al (2017) Effect of niobium oxide phase on the furfuryl alcohol dehydration. *Catal Commun* 97:65–69. <https://doi.org/10.1016/j.catcom.2017.04.019>
44. Kitano T, Okazaki S, Shishido T et al (2012) Brønsted acid generation of alumina-supported molybdenum oxide calcined at high temperatures: characterization by acid-catalyzed reactions and spectroscopic methods. *J Phys Chem C* 116:11615–11625. <https://doi.org/10.1016/j.molcata.2013.01.019>
45. Kitano T, Shishido T, Teramura K, Tanaka T (2012) Brønsted acid property of alumina-supported niobium oxide calcined at high temperatures: characterization by acid-catalyzed reactions and spectroscopic methods. *J Phys Chem C*. <https://doi.org/10.1021/jp3032429>
46. Jiao H, Zhao X, Lv C et al (2016) Nb₂O₅-γ-Al₂O₃ nanofibers as heterogeneous catalysts for efficient conversion of glucose to 5-hydroxymethylfurfural. *Sci Rep* 6:34068. <https://doi.org/10.1038/srep34068>
47. Everett DH (1972) Manual of symbols and terminology for physicochemical quantities and units. Appendix II: definitions, terminology and symbols in colloid and surface chemistry. Part I *Pure Appl Chem* 31:578–638
48. Suppino RS, Landers R, Cobo AJG (2016) Influence of noble metals (Pd, Pt) on the performance of Ru/Al₂O₃ based catalysts for toluene hydrogenation in liquid phase. *Appl Catal A* 525:41–49. <https://doi.org/10.1016/j.apcata.2016.06.038>
49. Okazaki S, Kurimata M, Iizuka T, Tanabe K (1987) The effect of phosphoric acid treatment on the catalytic property of niobic acid. *Bull Chem Soc Jpn* 60:37–41. <https://doi.org/10.1246/bcsj.60.37>
50. Ohuchi T, Miyatake T, Hitomi Y, Tanaka T (2007) Liquid phase photooxidation of alcohol over niobium oxide without solvents. *Catal Today* 120:233–239. <https://doi.org/10.1016/j.cattod.2006.07.044>
51. Medeiros FFP, Moura MFV, da Silva AGP et al (2006) The thermal decomposition of monohydrated ammonium oxotris (oxalate) niobate. *Brazilian J Chem Eng* 23:531–538. <https://doi.org/10.1590/S0104-66322006000400011>
52. Su TT, Zhai YC, Jiang H, Gong H (2009) Studies on the thermal decomposition kinetics and mechanism of ammonium niobium oxalate. *J Therm Anal Calorim* 98:449–455. <https://doi.org/10.1007/s10973-009-0300-4>
53. Li X, Zhao R, Sun B et al (2014) Fabrication of a-Fe₂O₃-g-Al₂O₃ core-shell nanofibers and their Cr(VI) adsorptive properties. *RSC Adv* 4:42376–42382. <https://doi.org/10.1039/c4ra03692a>
54. Arunkumar P, Ashish AG, Babu B et al (2015) Nb₂O₅/graphene nanocomposites for electrochemical energy storage. *RSC Adv*. <https://doi.org/10.1039/c5ra07895d>
55. Wachs IE, Jehng JM, Hardcastle FD (1989) The interaction of V₂O₅ and Nb₂O₅ with oxide surfaces. *Solid State Ionics* 32–33:904–910. [https://doi.org/10.1016/0167-2738\(89\)90374-3](https://doi.org/10.1016/0167-2738(89)90374-3)
56. Jehng J-M, Wachs Israel E (1990) Niobium oxalate. *Nov Mater Heterog Catal* 437:232–242
57. Kitano T, Shishido T, Teramura K, Tanaka T (2013) Characterization of thermally stable Brønsted acid sites on alumina-supported niobium oxide after calcination at high temperatures. *ChemPhysChem* 14:2560–2569. <https://doi.org/10.1002/cphc.201300189>
58. de Pietre MK, Almeida LCP, Landers R et al (2010) H₃PO₄- and H₂SO₄-treated niobic acid as heterogeneous catalyst for methyl ester production. *React Kinet Mech Catal* 99:269–280
59. Garbassi F, Bart J CJ, Petrini G (1981) XPS study of tellurium—niobium and tellurium—tantalum oxide systems. *J Electron Spectrosc Relat Phenom* 22:95–107
60. Paparazzo E (1987) XPS and Auger spectroscopy studies on mixtures of the oxides SiO₂, Al₂O₃, Fe₂O₃ and Cr₂O₃. *J Electron Spectrosc Relat Phenom* 43:97–112
61. Maciver DS, Tobin HH, Barth RT (1963) Catalytic aluminas I. surface chemistry of eta and gamma alumina. *J Catal* 2:485–497. [https://doi.org/10.1016/0021-9517\(63\)90004-6](https://doi.org/10.1016/0021-9517(63)90004-6)

62. Berteau P, Delmon B (1989) Modified aluminas: relationship between activity in 1-butanol dehydration and acidity measured by NH_3 TPD. *Catal Today* 5:121–137. [https://doi.org/10.1016/0920-5861\(89\)80020-3](https://doi.org/10.1016/0920-5861(89)80020-3)
63. García-Sancho C (2014) Catalizadores ácidos basados en Nb_2O_5 para procesos sostenibles en biorrefinerías: producción de biodiésel, acroleína y furfural. Universidad de Málaga, Málaga
64. Bernal HG, Galletti AMR, Garbarino G et al (2015) NbP catalyst for furfural production: FTIR studies of surface properties. *Appl Catal A* 502:388–398. <https://doi.org/10.1016/j.apcata.2015.06.031>
65. Zhang J, Zhuang J, Lin L et al (2012) Conversion of D-xylose into furfural with mesoporous molecular sieve MCM-41 as catalyst and butanol as the extraction phase. *Biomass Bioenerg* 39:73–77. <https://doi.org/10.1016/j.biombioe.2010.07.028>
66. Sener C, Motagamwala AH, Alonso DM, Dumesic JA (2018) Enhanced furfural yields from xylose dehydration in the γ -valerolactone/water solvent system at elevated temperatures. *Chemsuschem* 11:2321–2331. <https://doi.org/10.1002/cssc.201800730>
67. Parejas A, Montes V, Hidalgo-carrillo J et al (2017) Catalysts for the liquid-phase dehydration of xylose to furfural. *Molecules* 22:2257–2275. <https://doi.org/10.3390/molecules22122257>

Publisher's Note Springer Nature remains neutral with regard to jurisdictional claims in published maps and institutional affiliations.